




Two Nonlocal Variational Models for Retinex Image Decomposition

Frank W. Hammond¹^a, Catalina Sbert²^b and Joan Duran²^c

¹Higher Polytechnic School, University of the Balearic Islands, Spain

²Department of Mathematics and Computer Science & IAC3, University of the Balearic Islands, Cra. de Valldemossa, km. 7.5, E-07122 Palma, Illes Balears, Spain

Keywords: Retinex Theory, Illumination, Reflectance, Image Decomposition, Low-Light Enhancement, Variational Method, Total Variation, Nonlocal Regularization.

Abstract: Retinex theory assumes that an image can be decomposed into illumination and reflectance components. In this work, we introduce two variational models to solve the ill-posed inverse problem of estimating illumination and reflectance from a given observation. Nonlocal regularization exploiting image self-similarities is used to estimate the reflectance, since it is assumed to contain fine details and texture. The difference between the proposed models comes from the selected prior for the illumination. Specifically, Tychonoff regularization, which promotes smooth solutions, and the total variation, which favours piecewise constant solutions, are independently proposed. A comprehensive theoretical analysis of the resulting functionals is presented within appropriate functional spaces, complemented by an experimental validation for thorough examination.

1 INTRODUCTION

The Retinex theory (Land and McCann, 1971) aims to explain and simulate how the human visual system perceives color independently of global illumination changes. Accordingly, an image can be decomposed into luminance and reflectance components.

Many implementations of Retinex have been proposed in the literature. Based on the center/surround alternative algorithm (Land, 1986), Jobson et al. (Jobson et al., 1996; Jobson et al., 1997) introduced a method that filters the input image with Gaussian kernels, taking the low-frequency result as the illumination and the residual image as the reflectance. In (Horn, 1974; Morel et al., 2010), the Poisson equation is used to perform the decomposition.


Decomposing an image into illumination and reflectance is mathematically ill-posed, thus prior knowledge on the solution needs to be assumed. The regularization theory assumes that the image which is to be reconstructed is sufficiently smooth. In the variational framework, this is formulated through the minimization of functionals that induce a high energy when the priors are not fulfilled.


Kimmel et al. (Kimmel et al., 2001) pioneered a


variational model to estimate the illumination, which is assumed to be spatially smooth, in a multiscale setting. The reflectance is not considered and needs to be computed in post-processing. Guo et al. (Guo et al., 2017) infer the illumination as the minimizer of a simple energy functional that incorporates the total variation (TV) seminorm as regularization term (Rudin et al., 1992). The reflectance is obtained by pixelwise division between the input image and the estimated illumination. However, this approach tends to amplify the noise, especially in dark regions. To overcome this issue, the use of denoising techniques becomes essential. Ng and Wang (Ng and Wang, 2011) estimate illumination and reflectance simultaneously, penalizing gradient oscillations in the illumination through L^2 norm and using TV for the reflectance, which is thus assumed to be piecewise constant.

Many other variational methods perform the decomposition in the logarithmic domain. In this setting, Fu et al. (Fu et al., 2016) proposed a weighted gradient-based variational model to avoid issues when either the reflectance or the illumination is small.

Recently, an increasing number of deep learning methods with different architectures have been proposed (Chen et al., 2018; Wu et al., 2022). However, these approaches are less flexible and interpretable than model-based methods, and the training and testing of the networks require high computational costs.

^a <https://orcid.org/0009-0005-6890-0202>

^b <https://orcid.org/0000-0003-1219-4474>

^c <https://orcid.org/0000-0003-0043-1663>

In this paper, we propose two variational models to simultaneously estimate the illumination and reflectance components of an image. In both cases, non-local regularization exploiting image self-similarities is used to estimate the reflectance, since it is assumed to contain fine details and texture. For the illumination, Tychonoff regularization, favouring smooth solutions, and TV, favouring piecewise constant solutions, are independently proposed. A comprehensive study of the existence and uniqueness of minimizers in suitable functional spaces is provided.

The rest of the paper is organized as follows. In Section 2, we present the nonlocal spaces and display some tools from nonlocal vector calculus. Section 3 is devoted to the proposed models, where we prove the existence and uniqueness of minimizer and introduce the saddle-point formulations that will be used to compute the solutions through the first-order primal-dual algorithm by Chambolle and Pock (Chambolle and Pock, 2011). Section 4 evaluates the performance of the proposed methods and compares them with some state-of-the-art techniques. Finally, conclusions are drawn in Section 5.

2 NONLOCAL THEORY

TV assumes that images consist of connected smooth regions (objects) surrounded by sharp contours. Accordingly, it is optimal to reduce noise and reconstruct the main geometry, but it fails to preserve fine details. On the contrary, nonlocal regularization (Gilboa and Osher, 2009; Duran et al., 2014) allows any point to interact directly with any other point in the domain. The resemblance between them is usually evaluated by comparing a patch around each point. Thus, the underlying assumption is that images are self-similar, thereby preserving fine details and texture.

In this section, we introduce weighted L^p spaces, for which nonlocal regularization is well defined, and formalize a systematic and coherent framework for nonlocal operators. Let Ω be a finite-measure subset of \mathbb{R}^n , with $n \geq 2$, and $w: \Omega \rightarrow [0, +\infty)$ a bounded measurable function that is nonzero a.e. in Ω .

2.1 Weighted L^p Spaces

Let $p \in [1, +\infty]$. We define the weighted L^p space as

$$L^p_w(\Omega) = \left\{ f: \Omega \rightarrow \mathbb{R} : \int_{\Omega} (|f|^p w) dx < +\infty \right\},$$

which is endowed with the norm $\|f\|_{p,w} = \|fw^{1/p}\|_p$. Note that, in order $\|\cdot\|_{p,w}$ to be a norm, w must be nonzero a.e. in Ω , otherwise it will be a seminorm.

It is easy to show that $L^p_w(\Omega)$ is a Banach space containing $L^p(\Omega)$, for $p \in [1, +\infty]$. We are interested in $L^2_w(\Omega)$, which is a Hilbert space equipped with the scalar product $\langle f, g \rangle_{2,w} = \langle f\sqrt{w}, g\sqrt{w} \rangle_2 = \int_{\Omega} fgw dx$.

Definition 2.1. We define the *difference function* of $u \in L^p(\Omega)$ as $\hat{u}(x, y) = u(y) - u(x)$.

Note that $\|\hat{u}\|_p \leq 2|\Omega|^{1/p}\|u\|_p$, where the norm on the left is the $L^p(\Omega \times \Omega)$ -norm and the one on the right is the $L^p(\Omega)$ -norm. Therefore, $\hat{u} \in L^p(\Omega \times \Omega)$.

Proposition 2.1. Let $\{u_n\}_{n \in \mathbb{N}}$ be a sequence in $L^2(\Omega)$ converging weakly to u in $L^2(\Omega)$. Then, $\{\hat{u}_n\}_{n \in \mathbb{N}}$ converges weakly to \hat{u} in $L^2_w(\Omega)$.

Proof. Since $L^2_w(\Omega \times \Omega)$ is a Hilbert space, we can identify f^* with some $f \in L^2_w(\Omega \times \Omega)$ such that $f^*(x) = \langle f, x \rangle$. We have

$$\langle f, \hat{u}_n \rangle_{2,w} = \int_{\Omega} \int_{\Omega} (u_n(y) - u_n(x))f(x, y)w(x, y) dx dy.$$

Let us define the functions $F(x) = \int_{\Omega} f(x, y)w(x, y) dy$ and $G(y) = \int_{\Omega} f(x, y)w(x, y) dx$. Then,

$$(F(x))^2 \leq |\Omega|M \int_{\Omega} f(x, y)^2 w(x, y) dy,$$

where M is an upper bound for w , so that $\int_{\Omega} (F(x))^2 dx \leq M|\Omega| \cdot \|f\|_{2,w}^2 < +\infty$. Thus, $F \in L^2(\Omega)$. Similarly, it can be proved that $G \in L^2(\Omega)$. It follows that $f^*(\hat{u}_n) \rightarrow \langle u, G \rangle_2 - \langle u, F \rangle_2 = f^*(\hat{u})$. \square

Corollary 2.2. Let $\{u_n\}_{n \in \mathbb{N}}$ be a sequence in $L^2(\Omega)$ converging weakly to u in $L^2(\Omega)$. Then,

$$\liminf_n \|\hat{u}_n\|_{2,w} \geq \|\hat{u}\|_{2,w}$$

Proof. It follows from previous result and weak lower semicontinuity of norms in a Banach spaces. \square

2.2 Basic Nonlocal Vector Calculus

The notion of directional derivative extends to the nonlocal case as $\partial_y u(x) = \hat{u}(x, y)\sqrt{w(x, y)}$. The *nonlocal gradient* is then defined as the vector of nonlocal derivatives, i.e., $\nabla_w u(x, y) = \partial_y u(x)$.

The *nonlocal divergence* is defined to satisfy the adjoint relation $\langle \nabla_w u, v \rangle_{2,\Omega \times \Omega} = \langle u, -\text{div}_w(v) \rangle_{2,\Omega}$. A sufficient condition for this is defining

$$\text{div}_w(v)(x) = \int_{\Omega} v(y, x)\sqrt{w(y, x)} - v(x, y)\sqrt{w(x, y)} dy.$$

3 PROPOSED MODELS

Let us assume that the observed image S defined on Ω is the product of the illumination $L \in (0, +\infty)$ and the

reflectance $R \in (0, 1)$. By transforming $S = R \cdot L$ into the logarithmic domain, we get

$$l = s + r, \quad (1)$$

where $l = \log(L)$, $s = \log(S)$ and $r = -\log(R)$. Based on (1), we introduce two nonlocal variational models to estimate l and r simultaneously, using nonlocal regularization for the reflectance, assumed to contain fine details and texture, and testing Tychonoff and TV for the luminance, assumed to be smooth.

To find a global optimal solution to the proposed minimization problems, we use the first-order primal-dual algorithm introduced in (Chambolle and Pock, 2011). Therefore, we rewrite each problem in a saddle-point formulation by introducing dual variables. The algorithm consists of alternating a gradient ascent in the dual variable, a gradient descent in the primal variable, and an over-relaxation for convergence purposes. The gradient steps are given in terms of proximity operators, which are defined for any proper convex function φ as $\text{prox}_{\tau\varphi}(x) = \arg \min_y \varphi(y) + \frac{1}{2\tau} \|x - y\|_2^2$. For all details on convex and functional analysis omitted in this section, we refer to (Brézis, 2011; Chambolle and Pock, 2016).

3.1 Nonlocal and Tychonoff Terms

We propose to estimate r and l as the minimizers of

$$E_1(r, l) = \|\widehat{r}\|_{2,w}^2 + \frac{\alpha}{2} \|\|\nabla l\|_2\|_2^2 + \frac{\beta}{2} \|l - r - s\|_2^2 + \frac{\gamma}{2} \|l\|_2^2 \quad (2)$$

where $\alpha, \beta, \gamma > 0$ are trade-off parameters. The last term is added for purely technical reasons and has no actual practical significance.

Theorem 3.1. Let $\Lambda = L^2(\Omega) \times W^{1,2}(\Omega)$ be the space of admissible functions and $s \in L^2(\Omega)$. There exists a unique $(r^*, l^*) \in \Lambda$ s.t. $E_1(r^*, l^*) = \inf_{(r,l) \in \Lambda} E_1(r, l)$.

Proof. Existence. We follow the direct method and a proof similar to that in (Ng and Wang, 2011).

It is easy to see that E_1 is proper and bounded below, thus $b = \inf_{(r,l) \in \Lambda} E_1(r, l) < \infty$. Let $\{(r_n, l_n)\} \subseteq \Lambda$ be such that $E_1(r_n, l_n) \rightarrow b$.

Since $E_1(r_n, l_n)$ is uniformly bounded, so are $\int_{\Omega} |\nabla l_n|^2$ and $\|l_n\|_2$, implying that $\{l_n\}$ is uniformly bounded in $W^{1,2}(\Omega)$. By the Rellich-Kondrachov theorem, there exists $l^* \in L^2(\Omega)$ such that $l_n \rightarrow l^*$ in $L^2(\Omega)$, and, up to a subsequence, $l_n \rightharpoonup l^*$ in $W^{1,2}(\Omega)$ due to the space being reflexive.

Furthermore, $\{r_n\}$ is uniformly bounded in $L^2(\Omega)$ as $\|r_n\|_2 \leq \|l_n - r_n - s\|_2 + \|s\|_2 + \|l_n\|_2$. Thus, there exists $r^* \in L^2(\Omega)$ s.t., up to a subsequence, $r_n \rightharpoonup r^*$ in $L^2(\Omega)$. By Proposition 2.1, $\widehat{r}_n \rightharpoonup \widehat{r}^*$ in $L_w^2(\Omega \times \Omega)$.

Finally, due to the weak lower semicontinuity of the norms, $b = \liminf_n E_1(r_n, l_n) \geq E_1(r^*, l^*) \geq b$, from which we deduce $E_1(r^*, l^*) = b$.

Uniqueness. It is a direct consequence of E_1 being strictly convex. \square

3.1.1 Saddle-Point Optimization

Let $\Lambda' = L^2(\Omega \times \Omega) \times (L^2(\Omega))^n$ and $K: \Lambda \rightarrow \Lambda'$ be the linear operator $K(r, l) = (\nabla_w r, \nabla l)$. We also consider $G: \Lambda \rightarrow [0, +\infty]$ and $F: \Lambda' \rightarrow [0, +\infty]$, respectively defined as $G(r, l) = \frac{\beta}{2} \|r - l - s\|_2^2 + \frac{\gamma}{2} \|l\|_2^2$ and $F(a, b) = \|a\|_2^2 + \frac{\alpha}{2} \|b\|_2^2$.

The minimization of (2) can be rewritten in a saddle-point formulation as

$$\min_{(r,l) \in \Lambda} \sup_{(a,b) \in \Lambda'} \langle (a, b), K(r, l) \rangle - F^*(a, b) + G(r, l),$$

where F^* denotes the convex conjugate of F .

In practice, the initial values of a sequence generated by an iterative algorithm may have errors due to arbitrary initialization, which can accumulate and lead to undesired results in the final image. To mitigate this, an additional constraint is introduced. Since $l = s + r$, with $r \geq 0$, then $l \geq s$. Therefore, it makes sense to impose both $r \geq 0$ and $l \geq s$.

Finally, the luminance l and the reflectance r are computed through the following Chambolle-Pock primal-dual iterates, that is, initialize over-relaxation variables $\tilde{r}_0 = r_0 = 0, \tilde{l}_0 = l_0 = s$, and update the dual variables as follows:

$$\left\{ \begin{array}{l} \left(\begin{array}{c} a_{n+1} \\ b_{n+1} \end{array} \right) = \text{prox}_{\sigma F^*} \left(\begin{array}{c} a_n + \sigma \nabla_w(\tilde{r}_n) \\ b_n + \sigma \nabla(\tilde{l}_n) \end{array} \right) \end{array} \right.$$

Then, update the primal variables, impose the constraints $r \geq 0, l \geq s$ and update the over-relaxation variables.

$$\left\{ \begin{array}{l} \left(\begin{array}{c} r_{n+1/2} \\ l_{n+1/2} \end{array} \right) = \text{prox}_{\tau G} \left(\begin{array}{c} r_n + \tau \text{div}_w(a_{n+1}) \\ l_n + \tau \text{div}(b_{n+1}) \end{array} \right) \\ r_{n+1} = \max(r_{n+1/2}, 0), \quad l_{n+1} = \max(l_{n+1/2}, s) \\ \tilde{r}_{n+1} = 2r_{n+1} - r_n, \quad \tilde{l}_{n+1} = 2l_{n+1} - l_n \end{array} \right.$$

The proximity operators involved are

$$\text{prox}_{\tau G} \left(\begin{array}{c} a \\ b \end{array} \right) = \left(\begin{array}{c} \frac{(\beta\tau + \gamma\tau + 1)a + \beta\tau b - \beta\tau(\gamma\tau + 1)s}{\beta\gamma\tau^2 + 2\beta\tau + \gamma\tau + 1} \\ \frac{\beta\tau a + (\beta\tau + 1)b + \beta\tau s}{\beta\gamma\tau^2 + 2\beta\tau + \gamma\tau + 1} \end{array} \right)$$

$$\text{prox}_{\sigma F^*} \left(\begin{array}{c} a \\ b \end{array} \right) = \left(\begin{array}{c} \frac{a}{1 + \sigma/2} \\ \frac{b}{1 + \sigma/\alpha} \end{array} \right)$$

3.2 Nonlocal and TV Terms

We take $s \in L^2(\Omega)$ and α, β, γ positive numbers, and consider the functional E_2 over $\Lambda = L^2(\Omega) \times$



Figure 1: Dataset used for the experiments.

$(\text{BV}(\Omega) \cap L^2(\Omega))$:

$$E_2(r, l) = \|\hat{r}\|_{2,w}^2 + \alpha \text{TV}(l) + \frac{\beta}{2} \|l - r - s\|_2^2 + \frac{\gamma}{2} \|l\|_2^2. \quad (3)$$

Theorem 3.2. There exists a unique $(r^*, l^*) \in \Lambda$ such that

$$E_2(r^*, l^*) = \inf_{r, l} E_2(r, l)$$

Proof. Existence. This proof is very similar to that of Theorem 3.1. E_2 is clearly a proper functional, and thus we can consider a minimizing sequence $E_2(r_n, l_n) \rightarrow b = \inf E_2$. Again, each of the additive terms of $E_2(r_n, l_n)$ will be uniformly bounded.

From Holder inequality it follows that $\|l_n\|_1 \leq |\Omega|^{1/2} \|l_n\|_2$ is uniformly bounded.

Therefore, $\{\text{TV}(l_n)\}_{n \in \mathbb{N}}$ and $\{\|l_n\|_1\}_{n \in \mathbb{N}}$ are uniformly bounded, whence $\{l_n\}_{n \in \mathbb{N}}$ is bounded in $\text{BV}(\Omega)$. Therefore, there exists some $l^* \in \text{BV}(\Omega)$ such that, up to a subsequence,

$$l_n \xrightarrow{L^1(\Omega)} l^* \text{ and } l_n \xrightarrow{L^2(\Omega)} l^* \in L^2(\Omega).$$

Because of the lower semicontinuity of norms in $\text{BV}(\Omega)$ and $L^2(\Omega)$,

$$\liminf_n \left(\alpha \text{TV}(l_n) + \frac{\gamma}{2} \|l_n\|_2^2 \right) \geq \alpha \text{TV}(l^*) + \frac{\gamma}{2} \|l^*\|_2^2$$

This, as in 3.1, implies that $E_2(r^*, l^*) = b$.

Uniqueness. Again, a direct consequence of the functional being strictly convex. \square

3.2.1 Saddle-Point Optimization

The same primal-dual algorithm as in the previous section is used. The problem obtained is

$$\min_{r, l} T(K(r, l)) + G(r, l),$$

with $K(r, l) = (\nabla_w r, \nabla l)$, $T(a, b) = \|a\|_2^2 + \alpha \|b\|_1$ and $G(r, l) = \frac{\beta}{2} \|l - r - s\|_2^2 + \frac{\gamma}{2} \|l\|_2^2$ is the same as in the Tychonoff functional. The algorithm used is very

similar, the only difference being that the dual variables are updated via the proximity operator of T^* :

$$\begin{cases} \left(\begin{array}{c} a_{n+1} \\ b_{n+1} \end{array} \right) = \text{prox}_{\sigma T^*} \left(\begin{array}{c} a_n + \sigma \nabla_w(\tilde{r}_n) \\ b_n + \sigma \nabla(\tilde{l}_n) \end{array} \right) \end{cases}$$

The proximity operator is computed as follows:

$$\text{prox}_{\sigma T^*} \left(\begin{array}{c} a \\ b \end{array} \right) = \left(\begin{array}{c} \frac{a}{1 + \sigma/2} \\ \frac{b}{\max(1, |b|/\alpha)} \end{array} \right)$$

3.3 Proposed Weights

For the nonlocal regularization term in both models, we need to select an appropriate weight function $w : \Omega \times \Omega \rightarrow [0, +\infty)$. We propose to use bilateral weights that consider both the spatial closeness between points and the similarity in the input image $S : \Omega \rightarrow \mathbb{R}^C$. This similarity is computed by considering a whole patch around each point and using the Euclidean distance across the color channels:

$$d_a(S(x), S(y)) = \int_{\Omega} G_a(z) |S(x+z) - S(y+z)|^2 dz,$$

where $|\cdot|$ denotes the Euclidean norm in \mathbb{R}^C and G_a is a Gaussian kernel of standard deviation $a \geq 0$.

The weights are defined as

$$w(x, y) = \frac{1}{\Gamma(x)} \exp \left(-\frac{|x-y|^2}{h_{\text{spt}}^2} - \frac{d_a(S(x), S(y))}{h_{\text{sim}}^2} \right), \quad (4)$$

where $h_{\text{spt}}, h_{\text{sim}} > 0$ are filtering parameters that control how fast the weights decay with increasing spatial distance or dissimilarity between patches, respectively, and $\Gamma(x)$ is the normalization factor

$$\Gamma(x) = \int_{\Omega} \exp \left(-\frac{|x-y|^2}{h_{\text{spt}}^2} - \frac{d_a(S(x), S(y))}{h_{\text{sim}}^2} \right) dy.$$

Note that $0 < w(x, y) \leq 1$ and $\int_{\Omega} w(x, y) dy = 1$, but the normalization factor breaks down the symmetry of w . In the end, the average made between very similar regions preserves the integrity of the image but reduces its small oscillations, which contain noise.

For computational purposes, the nonlocal regularization is limited to interact only between points at a certain distance. Accordingly, the weight distribution is in general sparse since a few nonzero values are considered. In this setting, let $\mathcal{N}(x)$ denote a neighbourhood around each $x \in \Omega$. Then, $w(x, y)$ is defined as in (4) if $y \in \mathcal{N}(x)$, and zero otherwise. The normalization factor is finally given by

$$\Gamma(x) = \int_{\mathcal{N}(x)} \exp \left(-\frac{|x-y|^2}{h_{\text{spt}}^2} - \frac{d_a(L(x), L(y))}{h_{\text{sim}}^2} \right) dy.$$



Figure 2: Visual impact of the trade-off parameters α and β in the proposed models for the *Papiervert* image. The estimated illumination maps are displayed in the first and third rows for (2) and (3), respectively. The corresponding reflectance components are displayed in the second and fourth rows for (2) and (3), respectively. Larger values of the regularization parameter α provide smoother illumination components, while the geometry and colors remain in the reflectance maps. We observe that the shadows due to lighting conditions are retained in the illumination components. Furthermore, the difference between the two proposed models is evident in the estimated illumination maps. The results from (2) tend to be isotropically smooth due to the use of a Tychonoff prior, while the results from (3) are piecewise constant, as expected from the TV.

In practice, the weight of the reference point is set to the maximum of the weights in the neighbourhood, $w(x,x) = \max\{w(x,y) : y \in \mathcal{N}(x)\}$. This setting avoids the excessive weighting of the reference point. Furthermore, G_a is not considered as it is only necessary when the size of $\mathcal{N}(x)$ is large.

4 ANALYSIS AND EXPERIMENTS

In this section, we analyze the performance of the proposed method for illumination and reflectance de-

composition. Figure 1 displays the images we used in all experiments: *Building* (Petro et al., 2014), *Lamp* (Guo et al., 2017), *Bookcase* (Wei et al., 2018), *Horses* (Petro et al., 2014) and *Papiervert* (Morel et al., 2010).

For our variational methods, we fix the following parameters throughout the experimental section: $\gamma = 10^{-5}$, $h_{\text{spt}} = 1.25$, $h_{\text{sim}} = 2.5$ and the number of iterations is set to 2000. We revert the logarithmic transformation by applying the exponential function to the outputs of the primal-dual algorithm.

In Figure 2 we display the decomposition results

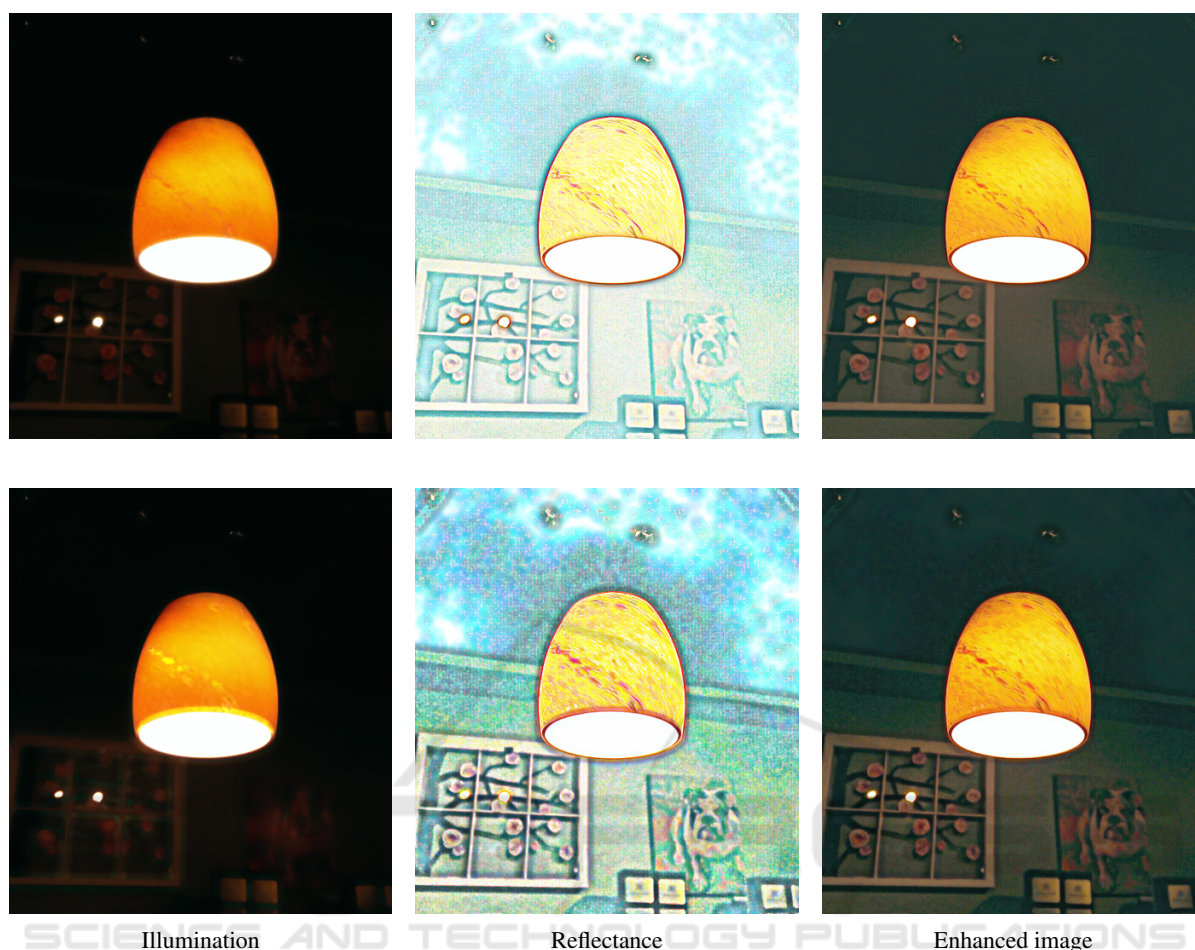


Figure 3: Resulting decomposition ($\alpha = 1, \beta = 5$) of *Lamp* by the proposed Tychonoff (2) (first row) and TV (3) (second row) models, and the respective enhanced images after applying a gamma correction with parameter 0.4 to the illumination component. We observe that the geometry, texture, color information, and noise are retained in the reflectance maps. Furthermore, the enhanced image by a simple gamma correction is able to discount the effect of the illumination in the scene. We also observe that the illumination map produced by Tychonoff is isotropically smooth while that of TV is piecewise constant.

for different α and β combinations in both models on *Papiervert*. Values were chosen taking into account that the nonlocal regularization term has a coefficient of 1 in both models. Thus, the smaller the values α, β are in relation to 1, the more importance is given to nonlocal regularization. In both models, bigger values for α tend to yield smoother results for illumination, which was to be expected since we are imposing that $|\nabla I|$ be small in the functional. Smaller values for α tend to yield illumination approximations that are very close to the original image, and reflectance approximations which are very close to $R = 1$. Bigger values for β tend to produce better results, since this parameter corresponds to our fidelity term. However, values too big ($\gg 20$, as experience indicates), tend to produce decompositions with the illumination approximation too close to the original image. We observe that the shadows due to lighting conditions

are retained in the illumination components. Furthermore, the difference between the two proposed models is evident in the estimated illumination maps. The results from (2) tend to be isotropically smooth due to the use of a Tychonoff prior, while the results from (3) are piecewise constant, as expected from the TV.

Experience shows that best results are often obtained for values of α and β smaller than 20, bigger than 1 and $\beta \geq \alpha$. We propose $\alpha = 1, \beta = 5$ as default parameters in both models.

In Figure 3, we show the decomposition of *Lamp* for our default combination $\alpha = 1$ and $\beta = 5$. A gamma correction of 0.4 is applied to illumination (although the corrected version is not displayed) before computing the resulting image.

In Figure 4, we compare the performance of our method with state-of-the-art techniques Multiscale Retinex (MSR) (Jobson et al., 1997), Kimmel et al.



Figure 4: Comparison between state-of-the-art techniques for low-light image enhancement and our models combined with a gamma correction to the illumination component. Each row contains the results by Kimmel et al., LIME, MSR, our Tychonoff model (2), and our TV model (3). Compared to our proposals, the method by Kimmel et al. produces similar results in terms of illumination, but is more sensitive to noise, LIME produces oversaturated colors, while MSR is not robust to noise and exhibits color issues. Our methods provide a good compromise between discounting the illumination, avoiding the amplification of noise, and preserving color and geometry. Note also that the results by Tychonoff are slightly more blurred than those of TV, as seen in the clouds and grass of *Horses* and on trees on *Building*.

(Kimmel et al., 2001) and LIME (Guo et al., 2017) on *Horses*, *Bookcase* and *Building*. The most suitable parameters for all methods have been chosen based on visual evaluation. We observe that neither MSR nor the method proposed by Kimmel et al. are robust to noise, LIME oversaturates color and MSR yields greyish images. In contrast, both our methods correctly enhance illumination, respect color and are relatively robust to noise. The Tychonoff model preserves color slightly better than TV, but contrasts are clearer in the latter.

5 CONCLUSION

In this paper, we proposed two variational models to simultaneously estimate the luminance and reflectance components from an observed image. Non-local regularization has been employed as a prior for the reflectance to help preserve colors and texture. Tychonoff and TV regularizations have been tested for the illumination component. We utilized this decomposition for low-light image enhancement.

In future work, it may be interesting to explore more sophisticated methods to enhance illumination and experiment with different mechanisms to reduce noise in our estimation of reflectance.

ACKNOWLEDGEMENTS

This work is part of the MaLiSat project TED2021-132644B-I00, funded by MCIN/AEI/10.13039/501100011033/ and by the European Union NextGenerationEU/PRTR, and also of the Mo-LaLIP project PID2021-125711OB-I00, financed by MCIN/AEI/10.13039/501100011033/FEDER, EU.

In memoriam Frank G. Hammond Figueroa.

REFERENCES

- Brézis, H. (2011). *Functional analysis, Sobolev spaces and partial differential equations*, volume 2. Springer.
- Chambolle, A. and Pock, T. (2011). A first-order primal-dual algorithm for convex problems with applications to imaging. *Journal of mathematical imaging and vision*, 40:120–145.
- Chambolle, A. and Pock, T. (2016). An introduction to continuous optimization for imaging. *Acta Numerica*, 25:161–319.
- Chen, W., Wenjing, W., Wenhan, Y., and Jiaying, L. (2018). Deep retinex decomposition for low-light enhancement. In *British Machine Vision Conference*.
- Duran, J., Buades, A., Coll, B., and Sbert, C. (2014). A nonlocal variational model for pansharpening image fusion. *SIAM Journal on Imaging Sciences*, 7(2):761–796.
- Fu, X., Zeng, D., Huang, Y., Zhang, X., and Ding, X. (2016). A weighted variational model for simultaneous reflectance and illumination estimation. *CVPR*, pages 2782–2790.
- Gilboa, G. and Osher, S. (2009). Nonlocal operators with applications to image processing. *Multiscale Modeling & Simulation*, 7(3):1005–1028.
- Guo, X., Yu, L., and Ling, H. (2017). Lime: Low-light image enhancement via illumination map estimation. *IEEE Transactions on Image Processing*, 26(2):982–993.
- Horn, B. K. (1974). Determining lightness from an image. *Computer Graphics and Image Processing*, 3(4):277–299.
- Jobson, D., Rahman, Z., and Woodell, G. (1996). Properties and performance of a center/surround retinex. *TIP*, 6(3):451–462.
- Jobson, D., Rahman, Z., and Woodell, G. (1997). A multi-scale retinex for bridging the gap between color images and the human observation of scenes. *IEEE Transactions on Image Processing*, 6(7):965–976.
- Kimmel, R., Elad, M., Shaked, D., Keshet, R., and Sobel, I. (2001). A variational framework for retinex. *Int. J. Comput. Vis.*, 52(1):7–23.
- Land, E. (1986). An alternative technique for the computation of the designator in the retinex theory of color vision. In *Proc. of the National Academy of Science*, volume 83 of 10, pages 3078–3080.
- Land, E. H. and McCann, J. J. (1971). Lightness and retinex theory. *Josa*, 61(1):1–11.
- Morel, J. M., Petro, A. B., and Sbert, C. (2010). A pde formalization of retinex theory. *IEEE Transactions on Image Processing*, 19(11):2825–2837.
- Ng, M. K. and Wang, W. (2011). A total variation model for retinex. *SIAM Journal on Imaging Sciences*, 4(1):345–365.
- Petro, A. B., Sbert, C., and Morel, J.-M. (2014). Multi-scale Retinex. *Image Processing On Line*, pages 71–88. <https://doi.org/10.5201/ipol.2014.107>.
- Rudin, L. I., Osher, S., and Fatemi, E. (1992). Nonlinear total variation based noise removal algorithms. *Physica D: nonlinear phenomena*, 60(1-4):259–268.
- Wei, C., Wang, W., Yang, W., and Liu, J. (2018). Deep retinex decomposition for low-light enhancement. *BMVC*.
- Wu, W., Weng, J., Zhang, P., Wang, X., Yang, W., and Jiang, J. (2022). Uretinex-net: Retinex-based deep unfolding network for low-light image enhancement. In *Proceedings of the IEEE/CVF conference on computer vision and pattern recognition*, pages 5901–5910.